

# Direct measurements of bar pattern speeds

E. M. Corsini

Dipartimento di Astronomia, Università di Padova, Padova, Italy  
e-mail: enricomaria.corsini@unipd.it

**Abstract.** The dynamics of a barred galaxy depends on the angular velocity or pattern speed of its bar. Indeed, it is related to the location of corotation where gravitational and centrifugal forces cancel out in the rest frame of the bar. The only direct method for measuring the bar pattern speed is the Tremaine-Weinberg technique. This method is best suited to the analysis of the distribution and kinematics of the stellar component in absence of significant star formation and patchy dust obscuration. Therefore, it has been mostly used for early-type barred galaxies. The main sources of uncertainties on the directly-measured bar pattern speeds are discussed. There are attempts to overcome the selection bias of the current sample of direct measurements by extending the application of the Tremaine-Weinberg method to the gaseous component. Furthermore, there is a variety of indirect methods which are based on the analysis of the gas distribution and kinematics. They have been largely used to measure the bar pattern speed in late-type barred galaxies. Nearly all the bars measured with direct and indirect methods end close to their corotation radius, i.e., they are as rapidly rotating as they can be.

**Key words.** galaxies: elliptical and lenticular, cD – galaxies: evolution – galaxies: kinematics and dynamics – galaxies: spiral – galaxies: structure

## 1. Introduction

Strong bars are observed in optical images of roughly half of all the nearby disk galaxies (Marinova & Jogee 2007; Barazza et al. 2008; Aguerri et al. 2009). Therefore bars are a common feature in the central regions of disk galaxies. Their growth is partly regulated by the exchange of angular momentum with the stellar disk and the dark matter halo. For this reason the dynamical evolution of bars can be used to constrain the content and distribution of dark matter in the inner regions of galaxy disks (e.g., Weinberg 1985; Bertin et al. 1989; Debattista & Sellwood 2000).

The morphology and dynamics of a barred galaxy depend on the angular velocity or pattern speed of the bar,  $\Omega_{\text{bar}}$ . Usually, the bar pattern speed is parametrized with the bar rotation rate  $\mathcal{R} \equiv R_{\text{CR}}/a_{\text{bar}}$ . This is the distance-independent ratio between the corotation radius  $R_{\text{CR}}$ , where the gravitational and centrifugal forces cancel out in the rest frame of the bar, and the length of bar semi-major axis  $a_{\text{bar}}$ . The corotation radius is derived from the bar pattern speed as  $R_{\text{CR}} = V_c/\Omega_{\text{bar}}$ , where  $V_c$  is the disk circular velocity. As far as the value of  $\mathcal{R}$  is concerned, if  $\mathcal{R} < 1.0$  the stellar orbits are elongated perpendicular to the bar and the bar dissolves. For this reason, self-consistent bars cannot exist in this regime. Bars with  $\mathcal{R} \gtrsim 1.0$

---

Send offprint requests to: Enrico Maria Corsini

are close to rotating as fast they can, and there is no a priori reason for  $\mathcal{R}$  to be significantly larger than 1.0.

The value of  $\mathcal{R}$  can be used to classify bars into fast ( $1.0 \leq \mathcal{R} \leq 1.4$ ) versus slow ( $\mathcal{R} > 1.4$ ), with the dividing value at 1.4 by consensus (Debattista & Sellwood 2000). Note the value of  $\mathcal{R}$  does not imply a specific value of the pattern speed.

## 2. Indirect methods for measuring the bar pattern speed

A variety of indirect methods has been used to measure the pattern speed of bars and their corresponding rotation rates. The identification of rings with the location of Lindblad's resonances (e.g., Vega Beltrán et al. 1998) and analysis of the offset and shape of dust lanes which trace the location shocks in the gas flows (Athanioula 1992; Puerari & Dottori 1997) promise to be simple and physically motivated methods to derive  $\Omega_{\text{bar}}$ . But, they are based on the correct interpretation of morphological features which are often elusive. The comparison of the observed gaseous kinematics to dynamical models of gas flow (e.g., Lindblad et al. 1996) and the comparison of the observed morphology to the predictions of numerical simulations (e.g., Rautiainen et al. 2008) combine both kinematic and photometric information. Furthermore, dynamical models can be applied to highly-inclined systems. But, both methods usually do allow to put strong constraints on the error budget and solution uniqueness.

In spite of being model-dependent, all the above methods give consistent results. The rotation rate of nearly all the measured bars is consistent to be  $1.0 \leq \mathcal{R} \leq 1.4$  within the errors (Elmegreen 1996; Rautiainen et al. 2008). However, the sample is biased toward late-type barred galaxies, because gas-rich systems are required for this kind of analysis.

## 3. The Tremaine-Weinberg method

Tremaine & Weinberg (1984, hereafter TW) suggested a model-independent way for measuring the bar pattern speed. They showed that

$\Omega_{\text{bar}}$  can be determined from readily observable quantities for a tracer population satisfying the continuity equation. It is

$$\Omega_{\text{bar}} \sin i = \frac{\int_{-\infty}^{+\infty} h(Y) dY \int_{-\infty}^{+\infty} V(X, Y) \Sigma(X, Y) dX}{\int_{-\infty}^{+\infty} h(Y) dY \int_{-\infty}^{+\infty} X \Sigma(X, Y) dX}, \quad (1)$$

where  $(X, Y)$  are the Cartesian coordinates in the sky plane, with the origin at the disk center and the  $X$  and  $Y$  axes aligned with the disk major and minor axes,  $h(Y)$  is an arbitrary weight function,  $\Sigma$  and  $V$  are the surface brightness and line-of-sight velocity of the tracer, and  $i$  is the disk inclination. The integration in  $X$  ranges over  $-\infty \leq X \leq +\infty$ , but integrating over  $-X_0 \leq X \leq X_0$  is sufficient if the disk is axisymmetric at  $|X| \geq X_0$ . Although the integration in  $Y$  ranges over  $-\infty \leq Y \leq +\infty$ , it is actually performed over an arbitrary range because of  $h(Y)$ . For example, a weight function proportional to a delta function  $\delta(Y - Y_0)$  corresponds to an aperture parallel to the disk major axis and offset by a distance  $Y_0$ . This is the case of the slits and pseudo-slits in long-slit and integral-field spectroscopy, respectively.

Merrifield & Kuijken (1995) refined the TW method. They suitably normalized both the numerator and denominator of the right-hand side of Eq. 1 with the total luminosity in the aperture. Thus, the TW equation takes the form

$$\Omega_{\text{bar}} \sin i = \frac{\langle V \rangle}{\langle X \rangle}, \quad (2)$$

where

$$\langle X \rangle = \frac{\int_{-\infty}^{+\infty} h(Y) dY \int_{-\infty}^{+\infty} X \Sigma(X, Y) dX}{\int_{-\infty}^{+\infty} h(Y) dY \int_{-\infty}^{+\infty} \Sigma(X, Y) dX} \quad (3)$$

and

$$\langle V \rangle = \frac{\int_{-\infty}^{+\infty} h(Y) dY \int_{-\infty}^{+\infty} V(X, Y) \Sigma(X, Y) dX}{\int_{-\infty}^{+\infty} h(Y) dY \int_{-\infty}^{+\infty} \Sigma(X, Y) dX} \quad (4)$$

are the luminosity-weighted means of the position and line-of-sight velocity of the tracer, respectively. Plotting  $\langle V \rangle$  versus  $\langle X \rangle$  for the different apertures produces a straight line with slope  $\Omega_{\text{bar}} \sin i$ , where the inclination of the

galaxy disk is known from the analysis of the surface-brightness distribution of the galaxy.

The assumption underlying the TW method is that the observed surface brightness is proportional to the surface density of the tracer, as for old stellar populations in the absence of significant star formation and patchy obscuration of dust. Thus, the method has been successfully applied to absorption-line spectra of early- and intermediate-type barred galaxies (Table 1). Extensions of the TW method were proposed to determine the distinct pattern speeds of two nested bars within a single galaxy (Corsini et al. 2003; Maciejewski 2006) and to measure a pattern speed which may vary arbitrarily with radius (Merrifield et al. 2006, see also Meidt, this volume).

Usually the presence of shocks, conversion of gas between different phases, and star formation on short timescales prevent the application of the TW method to gas. These limitations were explored by Rand & Wallin (2004) and Hernández et al. (2005) with numerical experiments. Ionized (Hernández et al. 2004, 2005; Emsellem et al. 2006; Fathi et al. 2007, 2009; Chemin & Hernandez 2009; Gabbasov et al. 2009), atomic (Bureau et al. 1999), and molecular gas (Zimmer et al. 2004; Rand & Wallin 2004) were used to derive the pattern speed of the bar (and/or spiral arms) in a growing number of intermediate- and late-type barred galaxies. The agreement between the bar parameters derived from the gas-based TW method and those obtained from indirect methods and numerical simulations suggests that although the gas does not obey the continuity equation, it can be used to derive the bar pattern speed. Nevertheless, a detailed estimate of the systematic effects due to departures from continuity and a comprehensive comparison with stellar-based TW measurements (and corresponding bar rotation rates) are still missing. Moreover, TW measurements of the same galaxy based on different tracers have been not performed yet. In the rest of this paper, I will focus on the application of the TW method to absorption-line spectra, while John E. Beckman will review the results obtained

from emission-line spectra in his contribution (this volume).

#### 4. Error budget

The main sources of uncertainties in TW measurements of  $\Omega_{\text{bar}}$  are summarized as follows.

*Centering errors:* The value of  $\Omega_{\text{bar}}$  can be significantly affected by small errors in identifying the position  $(X_C, Y_C)$  of galaxy center and in measuring the value  $V_{\text{sys}}$  of systemic velocity. This effect was already recognized by Tremaine & Weinberg (1984). To counter it, they suggested to adopt a weight function which is odd in  $Y$ , since barred galaxies are nearly point-symmetric about their centers. In long-slit spectroscopy the centering problem translates into one of fixing an arbitrary reference position and velocity frame common to all the slits. This in general is a much easier task to achieve. To this aim Merrifield & Kuijen (1995) rewrote Eq. 2 as

$$\Omega_{\text{bar}} \sin i = \frac{\langle V \rangle - V_{\text{sys}}}{\langle X \rangle - X_C}. \quad (5)$$

In integral-field spectroscopy the centering errors are minimized by the unambiguous determination of the common reference frame, which allows to know the exact position at which velocity and surface brightness of the tracer are measured.

*Signal-to-noise ratios:*  $\langle V \rangle$  and  $\langle X \rangle$  measure differences of velocity and luminosity across  $X = 0$ , respectively and are susceptible to the noise of available data. The signal-to-noise ratio of the spectral data can be increased by collapsing a long-slit spectrum along its spatial direction (Merrifield & Kuijen 1995) or by coadding all the spectra within a pseudo-slit (Debattista & Williams 2004). This produces a single one-dimensional spectrum with a high signal-to-noise ratio. The mean Doppler-shift of its absorption lines gives the  $\langle V \rangle$  value, which is required by the TW method. Broadband luminosity profiles have higher signal-to-noise ratios than luminosity profiles derived from spectra, particularly at large radii. Therefore, they can be adopted to compute the value of  $\langle X \rangle$  at each position of the slits or pseudo-slits (Aguerri et al. 2003).

**Table 1.** Barred galaxies with  $\Omega_{\text{bar}}$  measured by applying TW method to the stellar component

Galaxy (1)	Morp. Type (2)	$D$ (Mpc) (3)	$a_{\text{bar}}$ (kpc) (4)	$\Omega_{\text{bar}}$ (km s $^{-1}$ kpc $^{-1}$ ) (5)	$R_{\text{CR}}$ (kpc) (6)	$\mathcal{R}$ (7)	Ref. (8)
ESO 139-G09	(R)SAB0 $^0$ (rs)	71.9	$5.9^{+2.2}_{-1.0}$	$61 \pm 17$	$5.1^{+1.8}_{-1.1}$	$0.8^{+0.3}_{-0.2}$	A+03
ESO 281-G31	SB0 $^0$ (rs)	70.1	$3.7 \pm 0.3$	$31 \pm 12$	$6.8^{+4.1}_{-1.4}$	$1.8^{+1.1}_{-0.4}$	G+03
IC 874	SB0 $^0$ (rs)	34.7	$3.3^{+0.9}_{-0.8}$	$42 \pm 14$	$4.5^{+2.2}_{-1.1}$	$1.4^{+0.7}_{-0.4}$	A+03
NGC 271	(R')SBab(rs)	50.3	$7.1 \pm 0.2$	$32 \pm 18$	$10.7^{+7.3}_{-3.9}$	$1.5^{+1.0}_{-0.5}$	G+03
NGC 936	SB0 $^+$ (rs)	14.9	$3.6 \pm 0.4$	$66 \pm 15$	$5.0 \pm 1.1$	$1.4^{+0.5}_{-0.4}$	MK95
NGC 1023	SB0 $^-$ (rs)	5.8	$1.9 \pm 0.1$	$181 \pm 64$	$1.5^{+1.0}_{-0.6}$	$0.8^{+0.5}_{-0.3}$	D+02
NGC 1308	SB0/a(r)	82.4	$5.0^{+0.7}_{-1.4}$	$99 \pm 35$	$3.6^{+1.8}_{-0.9}$	$0.8^{+0.4}_{-0.2}$	A+03
NGC 1358	SAB0/a(r)	51.6	$4.8 \pm 0.8$	$37 \pm 18$	$5.8^{+4.8}_{-1.8}$	$1.2^{+1.0}_{-0.4}$	G+03
NGC 1440	(R')SB0 $^0$ (rs):	18.4	$2.2 \pm 0.5$	$82 \pm 19$	$3.4^{+1.0}_{-0.6}$	$1.6^{+0.5}_{-0.3}$	A+03
NGC 2523	SBbc(r)	46.0	$7.5 \pm 1.0$	$30 \pm 7$	$9.9^{+3.2}_{-1.9}$	$1.3^{+0.7}_{-0.5}$	T+07
NGC 2950	(R)SB0 $^0$ (r)	19.7	$3.3 \pm 0.2$	$117 \pm 25$	$3.1^{+0.8}_{-0.6}$	$1.0^{+0.3}_{-0.2}$	C+03
NGC 3412	SB0 $^0$ (s)	16.0	$2.4 \pm 0.2$	$57 \pm 16$	$3.6^{+1.3}_{-0.8}$	$1.5^{+0.6}_{-0.3}$	A+03
NGC 3992	SBbc(rs)	16.4	$4.5 \pm 1.0$	$72 \pm 5$	$3.6 \pm 0.2$	$0.8 \pm 0.2$	G+03
NGC 4245	SB0/a(r):	15.6	$2.9 \pm 0.4$	$62 \pm 25$	$3.2^{+2.2}_{-0.9}$	$1.1^{+1.1}_{-0.3}$	T+07
NGC 4431	dSB0/a	15.0	$1.6 \pm 0.1$	$102 \pm 26$	$0.9^{+0.3}_{-0.2}$	$0.6^{+0.2}_{-0.1}$	C+07
NGC 4596	SB0 $^+$ (r)	29.3	$7.5 \pm 1.1$	$28 \pm 7$	$8.6^{+2.8}_{-1.7}$	$1.1^{+0.7}_{-0.3}$	G+99
NGC 7079	SB0 $^0$ (s)	32.8	$4.0 \pm 0.6$	$53 \pm 1$	$4.9 \pm 0.2$	$1.2^{+0.3}_{-0.2}$	DW04

NOTE – Col.(2): Morphological classification from de Vaucouleurs et al. (1991, RC3), except for ESO 281-G31 (NASA/IPAC Extragalactic Database, NED) and NGC 4431 (Barazza et al. 2002). NGC 2950 is a double-barred galaxy and the listed values refer to its primary bar. Col.(3): Distance obtained as  $V_{\text{CBR}}/H_0$  with  $V_{\text{CBR}}$  from RC3, except for ESO 281-G31 (NED) and NGC 1308 (NED). The Hubble constant is assumed to be  $H_0 = 75 \text{ km s}^{-1} \text{ Mpc}^{-1}$ . Col.(4): Bar length from reference papers, except for NGC 936 (Kent & Glauzell 1989). Uncertainties of  $\pm 14\%$  (corresponding to the median error of the remaining galaxies) are assigned to the bar lengths of NGC 2523, NGC 4245, and NGC 4596, since errors are not quoted in the reference papers. Col.(5): Bar pattern speed from reference papers. Col.(6): Corotation radius from reference papers. Errors for NGC 2523 and NGC 4245 are not given in Treuthardt et al. (2007). Uncertainties are assigned according to the quoted errors on their pattern speeds. Col.(7): Bar rotation rate from reference papers. Uncertainties of NGC 936, NGC 2523, NGC 4245, and NGC 4596 are assigned according to quoted errors on bar length and corotation radius. Col.(8): Reference papers.

*Uncertainties on the disk position angle:* The TW method requires that the slits (or pseudo-slits) be exactly parallel to the disk major axis. A careful determination of the disk position angle  $\text{PA}_{\text{disk}}$  is therefore required before placing the slits or extracting the pseudo-slits. The maximum permitted misalignment between the position angle of the slits (or pseudo-slits) and  $\text{PA}_{\text{disk}}$  to have reliable  $\Omega_{\text{bar}}$  measurements depends on the galaxy inclination and bar orientation with respect the line of nodes (Debattista 2003). It ranges from  $1^\circ$  to

$4^\circ$  for  $\Delta\Omega_{\text{bar}}/\Omega_{\text{bar}} = 0.3$ . Galaxies with an inclination of about  $60^\circ$  and a bar at about  $20^\circ$  from the line of nodes on the disk plane are less sensitive to misalignment. The analysis of the galaxy isophotes mapped by deep imaging of the axisymmetric region of a disk gives  $\text{PA}_{\text{disk}}$  and  $i$ . Imaging is also useful to identify and discard target galaxies with structures (e.g., outer rings, spiral arms, warped or non-axisymmetric disks) which may interfere with the accurate measurement of  $\text{PA}_{\text{disk}}$  and  $i$  and affect the determination of  $\Omega_{\text{bar}}$ .

*Dust obscuration and star formation:* The TW method requires that the observed surface brightness of the tracer be proportional to its surface density. This is almost strictly satisfied by old stars in early-type disk galaxies, because they are characterized by slow star formation rate and low content of dust. Gerssen & Debattista (2007) investigated the effects of dust obscuration and star formation on the stellar-based TW measurements by means of numerical simulations. They find that  $\Delta\Omega_{\text{bar}}/\Omega_{\text{bar}} = 0.05$  for a diffuse disk of dust with a typically observed value of extinction  $A_V = 3$ . A unrealistically large  $A_V = 8$  gives  $\Delta\Omega_{\text{bar}}/\Omega_{\text{bar}} \leq 0.15$ . In addition, barred galaxies often display prominent dust lanes which run along the leading edges of the bar from the end of the bar toward the center of the galaxy (see Athanassoula 1992, for a morphological classification of dust lanes). Dust lanes tend to increase the TW-derived value of  $\Omega_{\text{bar}}$  when the position angle of the bar with respect to the disk major axis is  $\text{PA}_{\text{bar}} > 0^\circ$  and decrease it when  $\text{PA}_{\text{bar}} < 0^\circ$ . It is  $0.08 \leq \Delta\Omega_{\text{bar}}/\Omega_{\text{bar}} \leq 0.25$  for realistic dust lanes with  $A_V \approx 3$ . Including star formation does not affect these conclusions. These experiments show that it is possible to extend the application of the TW method to the stellar component of late-type barred galaxies (see also Gerssen & Debattista, this volume). The effects of dust obscuration could be further minimized by performing near-infrared spectroscopy.

*Number of slits (or pseudo-slits):* The value of  $\Omega_{\text{bar}} \sin i$  is derived by a straight-line fit to  $\langle X \rangle$  and  $\langle V \rangle$  data. They are measured along different slits (or pseudo-slits) crossing the galaxy bar and parallel to the disk major axis. Therefore, the accuracy of  $\Omega_{\text{bar}}$  determination depends also on the number of the observed slits (or pseudo-slits). It ranges from 2 (NGC 1358,  $\Delta\Omega_{\text{bar}}/\Omega_{\text{bar}} = 0.49$ ; Gerssen et al. 2003) to 9 (slits for the primary bar of NGC 2950,  $\Delta\Omega_{\text{bar}}/\Omega_{\text{bar}} = 0.21$ ; Corsini et al. 2003; pseudo-slits for NGC 7079,  $\Delta\Omega_{\text{bar}}/\Omega_{\text{bar}} = 0.02$ ; Debattista & Williams 2004). The most common case corresponds to 3 slits, they were measured for half of the sample galaxies. The comparison between  $\Delta\Omega_{\text{bar}}/\Omega_{\text{bar}}$  of NGC 2950 and NGC 7079 show

that  $\Delta\Omega_{\text{bar}}$  is dominated by the uncertainties on  $\langle X \rangle$  and  $\langle V \rangle$ . The median relative error on  $\Omega_{\text{bar}}$  is  $\Delta\Omega_{\text{bar}}/\Omega_{\text{bar}} = 0.27$ .

TW measurement of  $\Omega_{\text{bar}}$  requires no modeling. However, in the absence of gas velocities at large radii, the determination of  $\mathcal{R}$  requires some modeling to recover the disk circular velocity. The sources of uncertainties on  $\mathcal{R}$  are discussed hereafter.

*Uncertainties on the bar length:* Determining the length of a bar is not a entirely trivial task. This is particularly true for SB0 galaxies, for which there is no spiral structure or star formation beyond the bar marking its end. Moreover, the presence of a large bulge complicates further the measurement of  $a_{\text{bar}}$  (Aguerri et al. 2005). Several methods have been developed to derive the bar length (see Aguerri et al. 2009, for a list). Methods used to measure  $a_{\text{bar}}$  for the galaxies in Table 1 include: Fourier decomposition of galaxy light to analyze bar-interbar intensity ratio (Debattista et al. 2002; Aguerri et al. 2003; Gerssen et al. 2003; Corsini et al. 2003, 2007; Debattista & Williams 2004) or phase angle of Fourier mode  $m = 2$  (Aguerri et al. 2003; Gerssen et al. 2003; Corsini et al. 2003, 2007), study of the radial profile of ellipticity (Debattista et al. 2002) or phase angle of the deprojected ellipses which best fit galaxy isophotes (Debattista et al. 2002; Aguerri et al. 2003; Corsini et al. 2003, 2007), identification of a change in the slope of the surface-brightness profile along the bar major axis (Gerssen et al. 1999), visual inspection of galaxy images (Treuthardt et al. 2007), and decomposition of the surface-brightness distribution (Kent & Glaudell 1989; Kent 1990; Aguerri et al. 2003; Gerssen et al. 2003; Corsini et al. 2003, 2007). The relative error on the bar length for galaxies with at least two independent measurements is  $\Delta a_{\text{bar}}/a_{\text{bar}} < 0.25$  with a median  $\Delta a_{\text{bar}}/a_{\text{bar}} = 0.14$ . For each galaxy  $\Delta a_{\text{bar}}$  is assumed to be the average of the error intervals at 68% confidence level.

*Uncertainties on the corotation radius:* The corotation radius is obtained from the bar pattern speed and disk circular velocity. In the absence of gas which traces the circular velocity at large radii,  $V_c$  is recovered from the

observed streaming velocities, velocity dispersions, and light distribution of the stellar component by applying the asymmetric drift correction (see Binney & Tremaine 2008, p. 354). The difference between the stellar and circular velocity can be fairly large in the disks of bright SB0 galaxies ( $\Delta V/V = 0.2$ ), where large stellar velocity dispersions ( $\sigma \simeq 100 \text{ km s}^{-1}$ ) are observed (Debattista et al. 2002; Aguerri et al. 2003; Corsini et al. 2003). Relative error  $\Delta V_c/V_c$  ranges between 0.05 and 0.2 (with  $\Delta V_c$  defined as the average of 68% error intervals). It includes the scatter of the observed velocities in the flat portion of the stellar rotation curve and variation of the parameters adopted for the asymmetric drift correction. Uncertainties on the bar pattern speed and disk circular velocity translate into a relative error on the corotation radius as large as  $\Delta R_{\text{CR}}/R_{\text{CR}} = 0.57$  (NGC 1358; Gerssen et al. 2003). The median relative error of the sample is  $\Delta R_{\text{CR}}/R_{\text{CR}} = 0.28$  (with  $\Delta R_{\text{CR}}$  average of 68% error intervals).

## 5. Discussion and conclusions

All the bars in Table 1 are consistent with being fast (Fig. 1). This is particularly true when galaxies with small uncertainties on  $\mathcal{R}$  are considered. In fact, the probability that the bar length is twice as long as the corotation radius ( $\mathcal{R} > 2$ ) is 12% for all the sample galaxies and 8% for galaxies with  $\Delta \mathcal{R}/\mathcal{R} \leq 0.3$ . The median rotation rate is  $\mathcal{R} = 1.2$ . The fact that some of the values of bar rotation rate are nominally  $\mathcal{R} < 1$  has been interpreted by Debattista (2003) as due to the scatter introduced by uncertainties on  $\text{PA}_{\text{disk}}$ . The quoted uncertainties on  $\mathcal{R}$  are heterogeneous and include both 68% confidence intervals and maximal errors. It would be very useful if they were calculated and given in an homogeneous way. For example, they could be estimated from Monte Carlo simulations based on the uncertainties on  $a_{\text{bar}}$  and  $R_{\text{CR}}$ . No trend in  $\mathcal{R}$  is observed with morphological type. But, the sample of bars studied so far with the stellar-based TW method is biased toward the bright and strongly barred SB0 and SB0/a galaxies. One of them hosts two nested bars (NGC 2950, Corsini et al.

2003). The sample includes only 3 spiral galaxies (NGC 271, Gerssen et al. 2003; NGC 2523, Treuthardt et al. 2007; NGC 3992, Gerssen et al. 2003), and one dwarf galaxy (NGC 4431, Corsini et al. 2007).

The bar rotation rate of NGC 4431 is  $\mathcal{R} = 0.6^{+1.2}_{-0.4}$  at 99% confidence level (Corsini et al. 2007). Albeit with large uncertainty, the probability that the bar ends close to its corotation radius is about twice as likely as that the bar is much shorter than the corotation radius. This suggests a common formation mechanism of the bar in both bright and dwarf galaxies. If their disks were previously stabilized by massive dark matter halos, bars were not produced by tidal interactions because they would be slowly rotating (Noguchi 1999). But, this is not the case even in the two sample galaxies which show signs of weak tidal interaction with a close companion (i.e., NGC 1023, Debattista et al. 2002; NGC 4431, Corsini et al. 2007). There is no difference between TW measurements of the stellar component in isolated or mildly interacting barred galaxies. Besides, neither the length nor strength of the bars are found to be correlated with the local density of the galaxy neighborhoods (Aguerri et al. 2009).

The bars of ESO 139-G09 (Aguerri et al. 2003) and NGC 1358 (Gerssen et al. 2003) are weak and fast. Thus, the hypothesis of Kormendy (1979) that weak bars are the end state of slowed down fast bars is not supported by observations. They instead favor a scenario in which weak and strong bars form in the same way.

The  $\mathcal{R}$  determinations based on the stellar TW method agree with those obtained by indirect methods, which are largely adopted for gas-rich galaxies. According to the compilations by Elmegreen (1996) and Rautiainen et al. (2008), almost all the measured bars have  $1.0 \leq \mathcal{R} \leq 1.4$  within the errors. The same is true also for the  $\mathcal{R}$  values obtained from pattern speeds measured with the gas-based TW method (Bureau et al. 1999; Fathi et al. 2009; Chemin & Hernandez 2009). A fast bar is ruled out by errors only in NGC 2917 ( $\mathcal{R} > 1.7$ , Bureau et al. 1999) and UGC 628 ( $\mathcal{R} = 2.0^{+0.5}_{-0.3}$ , Chemin & Hernandez 2009). If bars of gas-

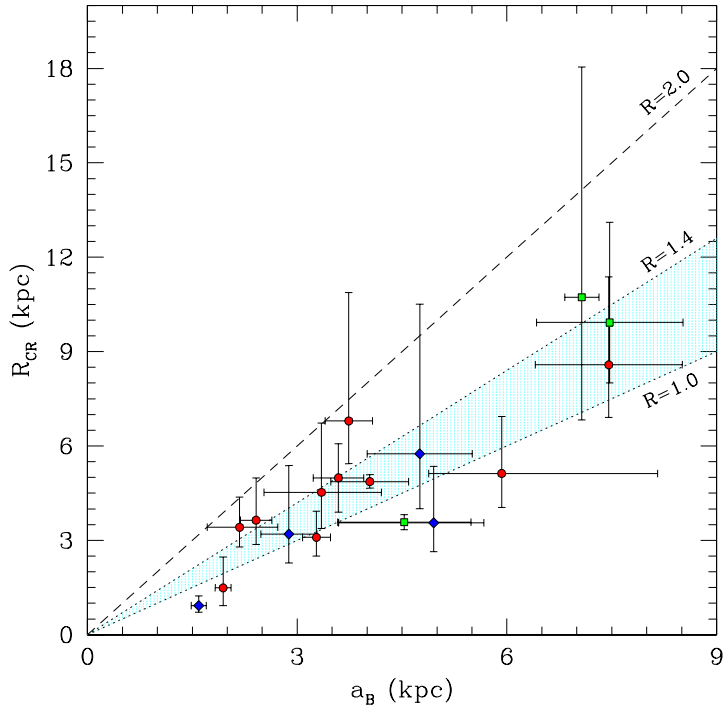


**Fig. 1.** The corotation radius  $R_{\text{CR}}$  as a function of the bar length  $a_{\text{bar}}$  for the barred galaxies with  $\Omega_{\text{bar}}$  measured by applying the stellar-based TW method. Red circles denote measurements for SB0 galaxies, blue diamonds correspond to SB0/a galaxies, and green squares represent spiral barred galaxies. The dotted lines correspond to  $\mathcal{R} = 1$  and  $\mathcal{R} = 1.4$ , respectively. They separate the forbidden ( $\mathcal{R} < 1$ ), fast-bar ( $1.0 \leq \mathcal{R} \leq 1.4$ , hatched area), and slow-bar ( $\mathcal{R} > 1.4$ ) regimes. The dashed line marks  $\mathcal{R} = 2$ .

poor lenticulars and early-type spirals have the same  $\mathcal{R}$  as gas-rich late-type spirals, then gas is not dynamically important for the evolution of bar pattern speed (Debattista 2003). Unfortunately, uncertainties on the measured  $\mathcal{R}$  are often not quoted for late-type galaxies. This missing piece of information is crucial to derive the  $\mathcal{R}$  distribution as a function of the morphological type.

Additional work is needed for the stellar TW method to increase both the accuracy of the  $\Omega_{\text{bar}}$  measurements and extend the number of studied late-type barred galaxies. Integral-field spectroscopy overcomes many problems of long-slit observations and leads to more efficient and accurate TW measurements. Dwarf barred galaxies are ideal targets to this aim.

They nicely fit the field of view of the available integral-field spectrographs and are good candidates for testing the predictions that dark-matter dominated barred galaxies should have a slow bar. A successful application of the TW method to the stellar component of late-type barred galaxies would remedy the selection bias present in the current sample of measured  $\Omega_{\text{bar}}$ . This will allow a straightforward comparison of the results of stellar-based TW method with indirect and gas-based TW measurements in the same range of Hubble types.

*Acknowledgements.* I would like to thank Victor Debattista for careful reading of the manuscript and comments that helped to improve it. I would also like to thank Alfonso Aguerri, John Beckman, and Lorenzo Morelli for their suggestions. This research

has been made possible by support from Padua University through grant CPDR095001. It has made use of the Lyon Extragalactic Database (LEDA) and NASA/IPAC Extragalactic Database (NED).

## References

- Aguerri, J. A. L., Debattista, V. P., & Corsini, E. M. 2003, MNRAS, 338, 465 (A+03)
- Aguerri, J. A. L., Elias-Rosa, N., Corsini, E. M., & Muñoz-Tuñón, C. 2005, A&A, 434, 109
- Aguerri, J. A. L., Méndez-Abreu, J., & Corsini, E. M. 2009, A&A, 495, 491
- Athanassoula, E. 1992, MNRAS, 259, 345
- Barazza, F. D., Binggeli, B., & Jerjen, H. 2002, A&A, 391, 823
- Barazza, F. D., Jogee, S., & Marinova, I. 2008, ApJ, 675, 1194
- Bertin, G., Lin, C. C., Lowe, S. A., & Thurstans, R. P. 1989, ApJ, 338, 78
- Binney, J., & Tremaine, S. 2008, Galactic Dynamics, 2nd ed. (Princeton Univ. Press, Princeton)
- Bureau, M., Freeman, K. C., Pfitzner, D. W., & Meurer, G. R. 1999, AJ, 118, 2158
- Chemin, L., & Hernandez, O. 2009, A&A, 499, L25
- Corsini, E. M., Debattista, V. P., & Aguerri, J. A. L. 2003, ApJ, 599, L29 (C+03)
- Corsini, E. M., et al. 2007, ApJ, 659, L121 (C+07)
- Debattista, V. P. 2003, MNRAS, 342, 1194
- Debattista, V. P., & Williams, T. B. 2004, ApJ, 605, 714 (DW04)
- Debattista, V. P., & Sellwood, J. A. 2000, ApJ, 543, 704
- Debattista, V. P., Corsini, E. M., & Aguerri, J. A. L. 2002, MNRAS, 332, 65 (D+02)
- de Vaucouleurs, G., de Vaucouleurs, A., Corwin, H. G., Jr., et al. 1991, Third Reference Catalogue of Bright Galaxies (Springer, New York) (RC3)
- Elmegreen, B. 1996, in Barred Galaxies, IAU Coll. 157, ASP Conf. Ser. 91, ed. R. Buta, D. A. Crocker, & B. G. Elmegreen (ASP, San Francisco), 197
- Emsellem, E., et al. 2006, MNRAS, 365, 367
- Fathi, K., Toonen, S., Falcón-Barroso, J., et al. 2007, ApJ, 667, L137
- Fathi, K., Beckman, J. E., Piñol-Ferrer, N., et al. 2009, ApJ, 704, 1657
- Gabbasov, R. F., Repetto, P., & Rosado, M. 2009, ApJ, 702, 392
- Gerssen, J., & Debattista, V. P. 2007, MNRAS, 378, 189
- Gerssen, J., Kuijken, K., & Merrifield, M. R. 1999, MNRAS, 306, 926 (G+99)
- Gerssen, J., Kuijken, K., & Merrifield, M. R. 2003, MNRAS, 345, 261 (G+03)
- Hernández, O., Carignan, C., Amram, P., & Daigle, O. 2004, in Penetrating Bars through Masks of Cosmic Dust, ASSL Conf. Ser. 319, ed. D. L. Block et al. (Kluwer, Dordrecht), 781
- Hernández, O., Wozniak, H., Carignan, C., et al. 2005, ApJ, 632, 253
- Kent, S. M. 1990, AJ, 100, 377
- Kent, S. M., & Glaudell, G. 1989, AJ, 98, 1588
- Kormendy, J. 1979, ApJ, 227, 714
- Lindblad, P. A. B., Lindblad, P. O., & Athanassoula, E. 1996, A&A, 313, 65
- Maciejewski, W. 2006, MNRAS, 371, 451
- Marinova, I., & Jogee, S. 2007, ApJ, 659, 1176
- Merrifield, M. R., & Kuijken, K. 1995, MNRAS, 274, 933 (MK95)
- Merrifield, M. R., Rand, R. J., & Meidt, S. E. 2006, MNRAS, 366, L17
- Noguchi, M. 1999, ApJ, 514, 77
- Puerari, I., & Dottori, H. 1997, ApJ, 476, L73
- Rand, R. J., & Wallin, J. F. 2004, ApJ, 614, 142
- Rautiainen, P., Salo, H., & Laurikainen, E. 2008, MNRAS, 388, 1803
- Tremaine, S., & Weinberg, M. D. 1984, ApJ, 282, L5
- Treuthardt, P., Buta, R., Salo, H., & Laurikainen, E. 2007, AJ, 134, 1195 (T+07)
- Vega Beltrán, J. C., Zeilinger, W. W., Amico, P., et al. 1998, A&AS, 131, 105
- Weinberg, M. D. 1985, MNRAS, 213, 451
- Zimmer, P., Rand, R. J., & McGraw, J. T. 2004, ApJ, 607, 285